arXiv:1501.06953v1 [astro-ph.HE] 27 Jan 2015

Pair-Instability Supernovae of Fast Rotating Stars

Ke-Jung Chen

Department of Astronomy & Astrophysics, University of California, 1156 High St.
Santa Cruz, California 95064, USA
School of Physics and Astronomy, University of Minnesota, 116 Church St.
Minneapolis, Minnesota 55455, USA
kchen@ucolick.org

We present 2D simulations of pair-instability supernovae considering rapid rotation during their explosion phases. Recent studies of the Pop III star formation suggested that these stars could be born with a mass scale about 100 $M_\odot$ and with a strong rotation. Based on stellar evolution models, these massive Pop III stars might have died as highly energetic pair-instability supernovae. We perform 2D calculations to investigate the impact of rotation on pair-instability supernovae. Our results suggest that rotation leads to an aspherical explosion due to an anisotropic collapse. If the first stars have a 50% of keplerian rotational rate of the oxygen core before their pair-instability explosions, the overall ^{56}Ni production can be significantly reduced by about two orders of magnitude. An extreme case of 100% keplerian rotational rate shows an interesting feature of fluid instabilities along the equatorial plane caused by non-synchronized and non-isotropic ignitions of explosions, so that the shocks run into the in-falling gas and generate the Richtmyer–Meshkov instability.

Keywords: stars: supernovae – nuclear reactions – stars: Population III – fluid instabilities

PACS Nos.: include PACS Nos.

1. Introduction

The first generation of stars so-called, Population III (Pop III) stars were predicted to form about several hundred million years after the Big Bang [1, 2]. The Pop III stars were born in the gravitational-potential wells constructed by the dark matter halos of masses about 10^6 solar masses ($M_\odot$), that allowed the primordial gas (mass content: 76 % hydrogen, 24% helium) to form stars. Because no heavy elements (metals) were present at that time, molecular hydrogen served as the most efficient coolant, but it could not cool the gas temperature efficiently. Thus, the Jeans mass of the Pop III star-forming cloud was expected to be much larger than the one of the current star formation regions; consequently the Pop III stars could be more massive than the present-day stars. Modern cosmology simulations suggested that the mass scale of the Pop III stars would fall between tens to hundreds of $M_\odot$. The exact mass scale is still under debate. Without initial metals such as carbon and oxygen, the Pop III stars needed to reach higher core temperatures to burn hydrogen effectively [3], that also resulted in higher surface temperatures. So these

stars could produce large amounts of UV photons and extensively ionized primordial hydrogen, and helium inside the inter-galactic medium (IGM) leading to the cosmic reionization [4, 5, 6, 7, 8]. After their short life time of several million years, many massive Pop III stars might have died as supernovae and dispersed the first metal to the primordial IGM. Such chemical enrichment might have changed the later star formation mode from Pop III to Pop II and profoundly reshaped the simple early universe into a state of ever-increasing complexity. Thus, understanding the first stars and their supernovae has become one of the frontiers of modern cosmology.

Fate of a massive star strongly correlate to its final mass before its death. Because there is no initial metal inside the envelope of Pop III stars, the mass loss rates due to the metal line-driven wind can be strongly suppressed. Hence, it is reasonable to assume that Pop III stars losses very little or no mass during their stellar evolution. Based on stellar physics [9, 10], the Pop III stars with initial masses of $10 - 80\, M_\odot$ eventually forge an iron core about one solar mass. When the iron core mass exceeds its Chandrasekhar mass [11], the degenerate pressure of electrons is no longer able to support its own gravity. The iron core catastrophically collapses into a black hole or neutron star. The energy released from the gravity allows an energetic explosion so-called a core-collapse supernova. However, such explosions may fail and the entire star may collapses directly into a black hole. The nature of core-collapse supernovae is complicated by several hurdles such as neutrino physics, multi-scale, and multi-dimension [12, 13, 14, 15, 16]. The explosion mechanisms remain subject to investigation. If Pop III stars are more massive than $80 M_\odot$. after the central carbon burning, their cores encounter the electron/positron production instability, the core reaches sufficiently high temperatures ($\sim 10^9\,$K) and low densities ($\sim 10^6\,$g cm^{-3}) to favor the creation of electron-positron pairs. It reduces the adiabatic index γ below $4/3$ and causes a dynamical instability of the core. The core is now at quasi hydrodynamical equilibrium and its temperatures begin to oscillate for a period of its dynamic time scale of several hundred seconds. The variations in temperature do not cause a significant impact to its evolution and the star later dies as a core-collapse supernova. However, if the stars are more than $100\,M_\odot$, the oscillation of temperatures becomes very violent. Several large temperature spikes produce shocks with energy of $10^{49} - 10^{50}$erg. These shocks can not disperse the entire star, but eject its outer envelopes instead. Due to different amount of mass and energetics, these ejected shells are likely to run into each other. The colliding shells effectively convert the kinetic energy of ejecta into the internal energy of gas. The collision sites usually happen at optically thin regions and thermal radiation escape immediately and produce very luminous optical transits known as pulsational pair-instability supernovae [17, 18]. Once the mass of stars reaches between 150 and 260 $M_\odot$. At this point, pair-instabilities become so violent and trigger a runaway collapse of core. The core temperature and density rise swiftly and ignite the explosive oxygen/silicon burning. The energy released from the burning converts the contraction of the core into an energetic explosion that completely disrupts the entire star. This thermonuclear explosion, known as a pair-instability supernova

(PSN), that has explosion energies up to 10^{53} erg and yield up to 50 $M_\odot$ of ^{56}Ni [19, 20, 21, 22, 23, 24, 25]. Most of Stars are 300 $M_\odot$ are believed to simply die as a black hole. A new type of supernova caused by the general-relativity instability in supermassive stars at $\sim 55,000$ $M_\odot$, which may have formed in the early universe, has now also been found [26].

Because the Pop III stars were predicted to very massive, many of them tended to die as PSNe. The 1D PSN models have been extensively studied by several authors [21, 22, 23, 27]. The extensive yields, explosion energies, and radiation properties of PSNe are calculated in their models. Unlike core-collapse supernovae, the thermonuclear explosions of PSNe are not very sensitive to the dimensionality of simulations. However, simulating the mixing of the fluid instabilities in PSNe still requires multidimensional simulations that recently become accessible and studied by [28, 24, 29, 18]. The simulations of [30] found the mixing of PSN from the both burning and hydrodynamics instabilities. In the red super-giant progenitors, the mixing driven by the Rayleigh-Taylor instabilities can be very significant.

One of the important physical quantities in the stellar evolution is rotation. In the real world, the process of star formation usually endows a certain amount of angular momentum to the star and makes it rotate. Due to the technical difficulty of the study, the rotational rates of massive stars are still poorly understood in both theoretical and observational studies. Rotation can affect the stellar evolution as well as the resulting supernova explosions. The nucleosynthesis inside the stars changes due to the rotational mixing, so that the chemical composition of the star changes. If metal from the inner part is mixed out to the envelope, the stellar wind can be enhanced due to metal-driven lines. Strong winds reduce the stellar mass dramatically and affect the fate of the stars. Studies of the stellar evolution of very massive stars with rotation have been performed by [20, 31, 32, 33, 34]. Recent results from [35, 36] show that rotation can lower the mass criterion for PSNe progenitors because mixing facilitates helium burning, resulting in a more massive oxygen core. Recent simulations [37] suggested that the Pop III stars could rotate very fast, up to 50 % of keplerian rate at the surface. If such a high rotation does exist, it can affect the evolution of the stars and their supernovae. So we perform 2D simulations of PSNe with rotation and investigate how the strong rotation impacts the explosive burning. The purpose of this paper is to explore the energetics and nucleosynthesis of PSNe during the explosion phase.

The structure of this paper is as follows: we first describe the numerical approaches and setup of our simulations in § 2. Then we present the results in § 3 and conclude our findings in § 4.

2. Methodology and Problem Setup

The 3D stellar evolution models followed from the main sequence star to supernovae are still unavailable due to the limitations of current computational power. Alternatively, we start simulating the stars with KEPLER [38, 39], a 1D spherically-symmetric

Lagrangian code, and follow the evolution of stars up to $20 - 100$ seconds before the supernova explosions. Then we map the resulting 1D stellar evolution models from KEPLER onto 2D grids of CASTRO as the initial conditions. We then apply our differential rotation scheme to CASTRO and follow the simulations until the explosive burning ceases when the shock has successfully launched. This setup is designed to model the most critical phases of the supernova explosion in 2D with practical computational resources. In this section, we introduce our progenitor models, problem setup, and numerical methods.

2.1. *Progenitor Models*

We use progenitor Pop III stars of $150\,M_\odot$, $200\,M_\odot$, and $250\,M_\odot$ with very little overshooting at the late-time evolution. These stars eventually become blue supergiants which have smaller radii than those of red supergiants. The 1D stellar models are evolved until most of the explosive burning is about to happen. Physical properties of these stars are listed in Table 1. The resulting 1D profiles are then mapped onto 2D cylindrical grids of CASTRO using a new mapping algorithm [40]. This initialization scheme conservatively maps the physical quantities such as mass and energy during mapping from 1D to multi-D. The initial perturbations are seeded in the form of velocities based on the stellar convection physics.

Table 1.   1D Progenitor models

Name	M_* $[M_\odot]$	M_{He} $[M_\odot]$	ρ_{c} $[10^6\,\mathrm{g\,cm}^{-3}]$	T_{c} $[10^9\,\mathrm{K}]$	R $[10^{13}\,\mathrm{cm}]$
B150	150	67	1.40	3.25	16.54
B200	200	95	1.23	3.31	2.86
B250	250	109	1.11	3.34	23.06

M_*: initial stellar mass; M_{He}: helium core mass at collapse; ρ_{c}: central density at collapse; T_{c}: central temperature at collapse; and R: stellar radius.

2.2. *CASTRO*

We run 2D simulations using CASTRO [41, 42], a massively parallel, multidimensional Eulerian, adaptive mesh refinement (AMR), hydrodynamics code for astrophysical applications. CASTRO was originally developed at the Lawrence Berkeley Lab, and it is designed to run effectively on supercomputers over 10,000 CPUs. CASTRO provides a powerful platform for simulating hydrodynamics and gravity for astrophysical gas dynamics. Modeling thermonuclear supernovae requires calculating the energy generation rates from nuclear burning, which occurs over an extensive range of temperatures, densities, and compositions of isotopes. We have implemented the APPROX 19-isotope reaction network [38, 43] into CASTRO. It is capable of efficiently calculating accurate energy generation rates for major nuclear reactions from hydrogen

to silicon burning. In CASTRO, we use a realistic equation of state (EOS) [44] for stellar matter. This EOS considers the (non)degenerate and (non)relativistic electrons, electron-positron pair production, as well as ideal gas with radiation. It is a tabular EOS that reads in ρ, T, and X_i of gas and yields its derivative thermodynamics quantities. CASTRO offers different types of calculation for gravity, including Constant, Poisson, and Monopole. For supernova simulations, spherical symmetry is still a good approximation for the mass distribution of gas at the early phase of evolution. Using this approximation saves lot of computational time in the gravity solver. For 2D or 3D CASTRO simulations, we first calculate a 1D radial average profile of density, then compute the 1D profile of $\mathbf{g}$ field and use it to calculate the gravity of the multidimensional grid cells. Care is taken to resolve the important scales of the explosions such as catching the shock front and mixing driven by fluid instabilities. The grid structure for 2D simulations uses base grids, 256×512 with additional three levels of AMR to resolve a domain of $(4 \times 10^{11}) \times (8 \times 10^{11})\,\mathrm{cm}^2$. This setup yields the size of the finest patch about $(7.2 \times 10^7)^2\,\mathrm{cm}^2$ which fully resolves the nuclear burning and the structures of fluid instabilities of rotating PSNe. The AMR criteria are set for gradients of density, velocity, and pressure. Finer zones are automatically created on the top of over-gradient regions. 2D CASTRO uses a cylindrical coordinate $r - z$. The axis z serves as the rotational axis. Since we simulate only half of the star in 2D. The lower boundary of r uses reflect conditions to prohibit fluid from entering; the other three boundaries use outflow conditions that allow the fluid to freely cross over. We also constructed nested zones to ensure that the inner region of the star constantly receives a higher spatial resolution.

2.3. *2D Rotational Model*

We develop a differential rotational model motivated by the stellar structure. It yields non-uniform rotational rates inside different regions of stars. Because the oxygen core of the star is a dense and compact object, we assume it behaves like a rigid body with a constant rotational rate, ω. Outside the oxygen core, the structure of the helium and hydrogen envelope is relatively puffy and unlikely to keep the constant ω. Instead, we assume a constant specific angular moment extending from the edge of oxygen core to its surface and ω monotonically decreases from the rotational axis, as shown in Figure 1. To determine the radius of oxygen core and its rotational rate, we plot the oxygen abundance as a function of radius in Figure 2(a). The most abundant oxygen is located at the radius between $10^9 - 10^{10}\,\mathrm{cm}$, and its outer boundaries of the oxygen core is at $10^{10}\,\mathrm{cm}$. Based on the size and mass of the oxygen core, we determine its keplerian rotational rates, ω_k which is about $0.5\,\mathrm{sec}^{-1}$. To examine whether the model is viable, we calculate ω_k as a function of radius in Figure 2(b). It shows a nice trend of constant ω in the the oxygen core and slowly decrease from the core boundary. Our assumption of oxygen rotating as a rigid body seems to be very suitable for the model.

We therefore assume a constant rotational rate inside the oxygen core and this
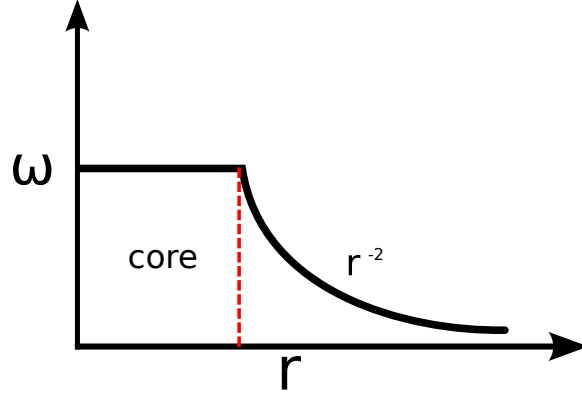
Fig. 1.   Illustration of the differential rotational model. ω is the rotational rate and r is the distance to the rotational axis. ω inside the oxygen core ($r \leq r_c$) is assumed as a constant. Beyond the core ($r > r_c$), we assume a specific angular j constant and result in $\omega \propto r^{-2}$.
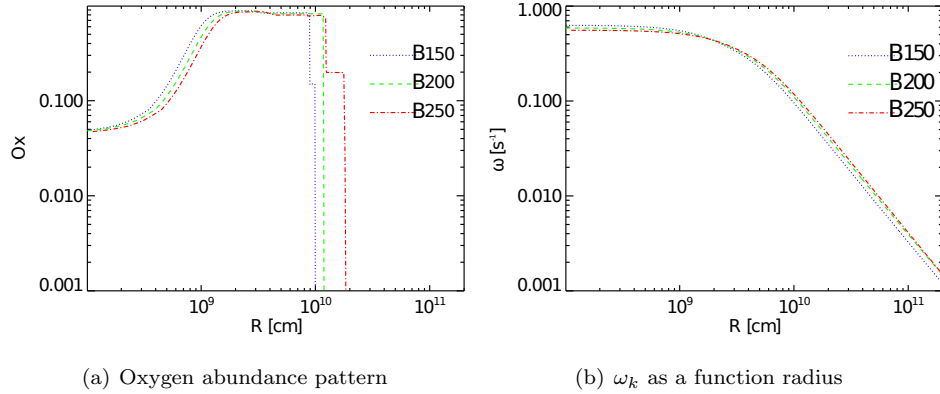

(a) Oxygen abundance pattern

(b) ω_k as a function radius

Fig. 2.   (a) The size of the oxygen cores of presupernovae can be identified by their oxygen abundance. The sudden drop in the oxygen core marks the size of oxygen core. (b) $\omega(r)$ behaves like a constant then decreases. The saddle point of the drop is roughly at the edge of oxygen core.

rate is based on the keplerian rate of the oxygen core. In `CASTRO`, the rotation is calculated by the angular momentum, j which provides a force term in the Euler equation for fluids and itself is evolved by advect equations:

$$\frac{\partial(\rho \mathbf{u})}{\partial t} = -\nabla \cdot (\rho \mathbf{u}\mathbf{u}) - \nabla p + \rho \mathbf{g} + \mathbf{F}_c, \tag{1}$$

$$\frac{\partial(\rho j)}{\partial t} = -\nabla \cdot (\rho \mathbf{u} j). \tag{2}$$

$$\mathbf{F}_c = \rho \frac{j^2}{r_z^3}; \quad j = \omega r^2 \text{ when } r \leq r_c, \text{ otherwise } j = \omega r_c^2 \tag{3}$$

Here $\rho, p, \mathbf{u}, \mathbf{g}$ are the density, pressure, velocity vector, and gravitational vector, respectively. $\mathbf{F}_c$ is the centrifugal force calculated by ρ, the angular momentum per unit mass j, and the distance to the rotational axis r_z. j is only initialized at the beginning of the simulations, then it evolves with fluid elements following the equations as above.

3. Results

We first present the results from the representative model of the $200\,M_\odot$ rotating Pop III star with $\omega = 0.5\omega_k$. After the onset of the 2D `CASTRO` simulation, the core of the star starts to collapse due to its dynamical instabilities caused by pair-production instabilities. Similar to the case of non-rotating stars, explosive oxygen and silicon burning proceed as the core contracts. After about 25 seconds, the energy released from the nuclear burning launches a shock and the core of star has successfully exploded. For a non-rotating case, collapse of the core is perfectly anisotropic and homogeneous. Thus, the resulting explosion appears to have spherical symmetry. However, for a rotating star, rotation provides a centrifugal force to resist the in-falling gas during the collapse. Because the centrifugal force follows as $\mathbf{F}_c \propto r_z\omega^2$, for the given distance from the center of star, the core receives the strongest $\mathbf{F}_c$ along the equatorial direction and no force in the polar direction. It automatically leads to anisotropic compression of the core and reflects in the explosion. The maximum compression happens along the polar direction and yields more explosion energy and releases a more powerful shock wave than other directions. The core is blew up in an elliptical shape with a long axis along the rotational axis. Figure 3 shows the post-explosion of $200\,M_\odot$ progenitor star, $\omega = 0$ in the left-half panel and $\omega = 0.5\omega_k$ in the right-half panel. Both snapshots are taken at the same time after the explosions occur. In comparison of both results, the non-rotating model shows a stronger shock wave, and demonstrates some mixing at the inner part of the oxygen-burning shells. The rotating model, however, shows a relatively less energetic explosion due to a weaker compression; the ejected oxygen-burning shell is shaped into an ellipse and shows very little mixing. PSNe of non-rotating stars usually produce a large amount of radioactive isotope, ^{56}Ni which is made inside PSNe mainly by the explosive ^{28}Si burning right before the core bounces. Because the decay energy from ^{56}Ni powers the PSN light curves, it becomes one of the key isotopes for observations. The amount of ^{56}Ni production can determine whether the PSNe become bright or faint SNe. We show the corresponding ^{56}Ni abundance and gas density in Figure 4. The non-rotating star demonstrate a visual ^{56}Ni abundance, which is missing in the rotating model. It suggests that ^{56}Ni production has been significantly suppressed due to rotation. Only about $10^{-2}\,M_\odot$ ^{56}Ni is made in the rotational model. However, the non-rotating model has synthesized about $6.57\,M_\odot$ of ^{56}Ni. This suggests that a strong rotation can significantly affect the energetic and ^{56}Ni production in PSNe .

What happens if $\omega = \omega_k$? This is an extreme rotational rate which can al-
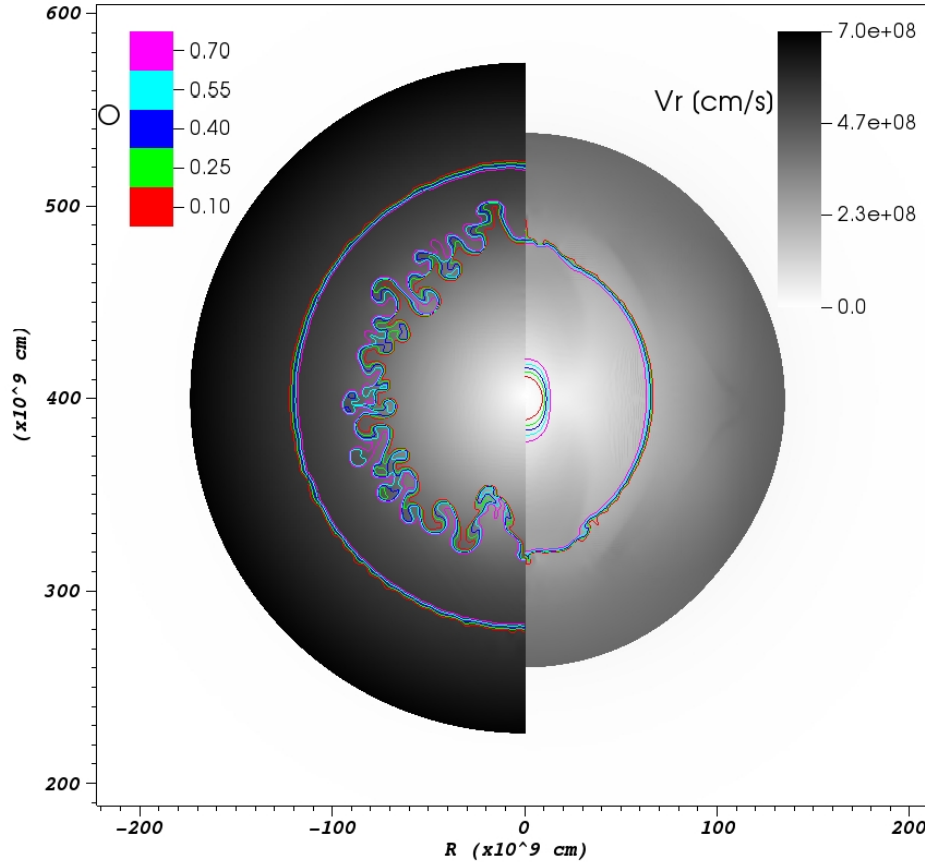
8   *Chen*

Fig. 3.   Comparison of rotating and non-rotating models from a 200 $M_\odot$ Pop III star. The left-half sphere is the non-rotating model, and the right-half is the rotating model of $\omega \sim 0.5\omega_k$. The gray colors show the radial velocities v_r, and the colorful contours are the ^{16}O mass fraction. Both snapshots are taken at the same time, about 200 sec after the onset of the explosion.

most break out of the star's core. To answer this question, we simulate a 200 $M_\odot$ of $\omega = \omega_k$. The anisotropic compression becomes even more stronger than that of the $\omega = 0.5\omega_k$ case. The ellipse shape of the ejected core has an larger eccentricity. One interesting fluid instability has been found in the carbon-burning shell, which is shown in Figure 5. The carbon shell breaks along the equatorial plane and over-shoots some carbon into the oxygen core. This overshooting develops strong fluid instabilities. Because the explosion is anisotropic, the shocks of different directions are initialized at different times: the pole comes first, and the equator comes last. In this fast-rotating model, the shock from the pole has been sent out, but the gas along the equator is still collapsing. Once the shock runs into the collapsing gas, the Richtmyer−Meshkov (RM) instability [45] starts to develop and the resulting mixing makes carbon penetrate into the oxygen-rich envelope.
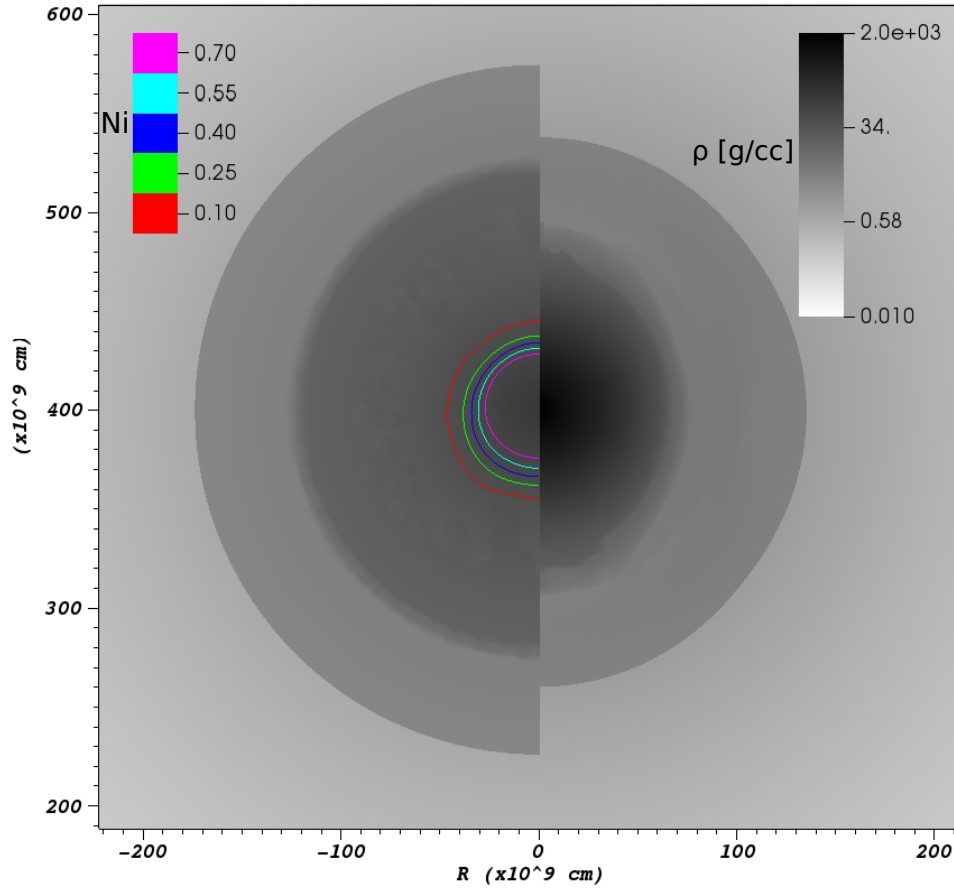
Fig. 4.   Comparison of rotating and non-rotating models from a 200 $M_\odot$ star. The left-side sphere is the non-rotating model, and the right side shows a rotating model of $\omega \sim 0.5\omega_k$. The gray color shows the density, and the colorful contours are the ^{56}Ni mass fraction. Both snapshots are taken at the same time, about 200 sec after the onset of the explosion.

4. Conclusions

Stellar rotation plays a key role in both stellar evolution and the fate of the very massive Pop III stars. The nature of the rotation can be traced back to the phase of star formation, when they are endowed with angular momentum. The definite rotational rates for the massive Pop III stars are still unknown. Results of these star formation suggest that a high rotational rate is 50% of its keplerian rotational rate. We present the results of the impact of rotation on a 200 $M_\odot$ star. The 50% keplerian rotational rate case demonstrates the onset of an anisotropic explosion and strongly suppresses ^{56}Ni. If this does apply for PSN progenitors, ^{56}Ni production shown in previous PSN models may change and the corresponding PSNe luminosity will be attenuated. An extreme case of a 100% keplerian rate shows an interesting feature of
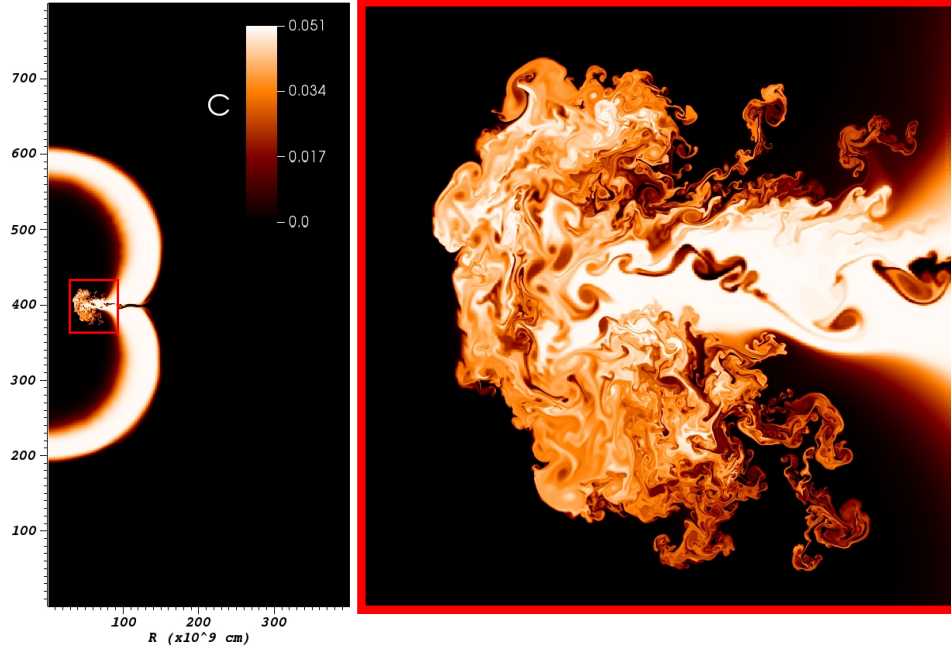
Fig. 5.   Hot-color shows the mass fraction of ^{12}C. Strong fluid instabilities occur during the explosion along the equatorial plane shown in the red box of the left panel; its close-up appears in the right panel.

overshooting along the equatorial plane caused by non-synchronized explosions that send shocks into the infilling gas. Finally, we conclude that PSNe of fast rotating stars would look much fainter than we originally expect because of the limited ^{56}Ni production.

Acknowledgments

References

1. T. Abel, G. L. Bryan and M. L. Norman, *Science* **295**, 93 (January 2002).
2. V. Bromm, N. Yoshida, L. Hernquist and C. F. McKee, *Nature* **459**, 49 (May 2009).

3. D. Schaerer, *A&A* **382**, 28 (January 2002).
4. B. J. Carr, J. R. Bond and W. D. Arnett, *ApJ* **277**, 445 (February 1984).
5. D. Whalen, T. Abel and M. L. Norman, *ApJ* **610**, 14 (July 2004).
6. T. Kitayama, N. Yoshida, H. Susa and M. Umemura, *ApJ* **613**, 631 (October 2004).
7. M. A. Alvarez and T. Abel, *MNRAS* **380**, L30 (September 2007).
8. T. Abel, J. H. Wise and G. L. Bryan, *ApJ* **659**, L87 (April 2007).
9. R. Kippenhahn and A. Weigert, *Stellar Structure and Evolution* 1990.
10. S. E. Woosley, A. Heger and T. A. Weaver, *Reviews of Modern Physics* **74**, 1015 (November 2002).
11. S. Chandrasekhar, *Principles of stellar dynamics* 1942.
12. A. Burrows, J. Hayes and B. A. Fryxell, *ApJ* **450**, 830 (September 1995).
13. H.-T. Janka and E. Mueller, *A&A* **306**, 167 (February 1996).
14. A. Mezzacappa, A. C. Calder, S. W. Bruenn, J. M. Blondin, M. W. Guidry, M. R. Strayer and A. S. Umar, *ApJ* **495**, 911 (March 1998).
15. J. W. Murphy and A. Burrows, *ApJ* **688**, 1159 (December 2008).
16. J. Nordhaus, A. Burrows, A. Almgren and J. Bell, *ApJ* **720**, 694 (September 2010).
17. S. E. Woosley, S. Blinnikov and A. Heger, *Nature* **450**, 390 (November 2007).
18. K.-J. Chen, A. Heger, S. Woosley, A. Almgren and D. J. Whalen, *ApJ* **792**, 44 (September 2014).
19. Z. Barkat, G. Rakavy and N. Sack, *Physical Review Letters* **18**, 379 (March 1967).
20. W. Glatzel, K. J. Fricke and M. F. El Eid, *A&A* **149**, 413 (August 1985).
21. A. Heger and S. E. Woosley, *ApJ* **567**, 532 (March 2002).
22. A. Heger and S. E. Woosley, *ApJ* **724**, 341 (November 2010).
23. D. Kasen, S. E. Woosley and A. Heger, *ApJ* **734**, 102 (June 2011).
24. K. Chen, A. Heger and A. S. Almgren, *Computer Physics Communications* **182**, 254 (January 2011).
25. K.-J. Chen, S. Woosley, A. Heger, A. Almgren and D. J. Whalen, *ApJ* **792**, 28 (September 2014).
26. K.-J. Chen, A. Heger, S. Woosley, A. Almgren, D. J. Whalen and J. L. Johnson, *ApJ* **790**, 162 (August 2014).
27. L. Dessart, R. Waldman, E. Livne, D. J. Hillier and S. Blondin, *MNRAS* **428**, 3227 (February 2013).
28. C. C. Joggerst and D. J. Whalen, *ApJ* **728**, 129 (February 2011).
29. E. Chatzopoulos and J. C. Wheeler, *ApJ* **760**, 154 (December 2012).
30. K.-J. Chen, *International Journal of Modern Physics D* **23**, 30008 (March 2014).
31. A. Maeder and G. Meynet, *ARA&A* **38**, 143 (2000).
32. A. Heger, S. E. Woosley and H. C. Spruit, *ApJ* **626**, 350 (June 2005).
33. R. Hirschi, *A&A* **461**, 571 (January 2007).
34. S. Ekström, G. Meynet, C. Chiappini, R. Hirschi and A. Maeder, *A&A* **489**, 685 (October 2008).
35. E. Chatzopoulos and J. C. Wheeler, *ApJ* **748**, 42 (March 2012).
36. S.-C. Yoon, A. Dierks and N. Langer, *A&A* **542**, A113 (June 2012).
37. A. Stacy, V. Bromm and A. Loeb, *MNRAS* **413**, 543 (May 2011).
38. T. A. Weaver, G. B. Zimmerman and S. E. Woosley, *ApJ* **225**, 1021 (November 1978).
39. A. Heger, S. E. Woosley, G. Martínez-Pinedo and K. Langanke, *ApJ* **560**, 307 (October 2001).
40. K.-J. Chen, A. Heger and A. S. Almgren, *Astronomy and Computing* **3**, 70 (November 2013).
41. A. S. Almgren, V. E. Beckner, J. B. Bell, M. S. Day, L. H. Howell, C. C. Joggerst, M. J. Lijewski, A. Nonaka, M. Singer and M. Zingale, *ApJ* **715**, 1221 (June 2010).

12   *Chen*

42. W. Zhang, L. Howell, A. Almgren, A. Burrows and J. Bell, *ApJS* **196**, 20 (October 2011).
43. F. X. Timmes, *ApJS* **124**, 241 (September 1999).
44. F. X. Timmes and F. D. Swesty, *ApJS* **126**, 501 (February 2000).
45. M. Brouillette, *Annual Review of Fluid Mechanics* **34**, 445 (2002).